S. Albatran
M. Alomoush

J. Electrical Systems x-x (xxx): x-xx

Regular paper

Modeling and Simulation of TCSC-Operated Single-Phase Induction Motor

As single-phase induction motor (SPIM) is not a self-starting motor, it has been a common practice to add an auxiliary component to the motor circuit to establish a starting torque. Traditionally, two capacitors are used in SPIM to establish and improve its starting torque and to enhance its running performance. As the Thyristor-Controlled Series Compensator (TCSC) is a control device that considerably alters impedance of the circuit in which it is inserted to be capacitive or inductive, it can be utilized for starting and running purposes in SPIM. This paper explores the representation of the TCSC as a variable impedance and investigates its valuable impacts, when it is operated in its capacitive mode, on the transient behavior of SPIM. It presents a state-space model of the TCSC-inserted SPIM and shows that inserting the TCSC in the auxiliary winding of the SPIM introduces more benefits compared to the traditionally used methods of starting and running the SPIM. The simulation results of the test cases presented in the paper, which include comparisons between the presented approach and the traditional approaches, emphasize that incorporating TCSC with the SPIM brings advantageous features to start and run the motor. The paper will show that controlling the firing angle of the TCSC may attain the desired electromagnetic torque and speed characteristics. The simulation results presented in the paper indicate that the TCSC can effectively replace the traditional auxiliary component and the accompanying mechanical centrifugal switch, which in turn may reduce the size and cost of the SPIM.

Keywords: Auxiliary Winding, Modeling and Simulation, Single-Phase Induction Motor, TCSC.
.

1. Nomenclature

v_{qs}, v_{ds}	The q-axis and d-axis stator voltages, respectively.
$v_{qr}^{'}, v_{dr}^{'}$	The q-axis and d-axis rotor voltages referred to stator windings, respectively.
i_{qs}, i_{ds}	The q-axis and d-axis stator currents, respectively.
$i_{qr}^{'}$, $i_{dr}^{'}$	The q-axis and d-axis rotor currents referred to stator windings, respectively
$\lambda_{qs}, \lambda_{ds}$	The q-axis and d-axis stator flux linkages, respectively.
$\lambda_{qr}^{'}, \lambda_{dr}^{'}$	The q-axis and d-axis rotor flux linkages referred to stator windings, respectively.
r_s, r_S	The q-axis and d-axis stator winding resistances, respectively.
$r_r^{'}$, $r_R^{'}$	The q-axis and d-axis rotor winding resistances referred to stator windings, respectively.

Corresponding author: M. Alomoush
Department of Electrical Power Engineering, Hijjawi Faculty for Engineering Technology, Yarmouk University, Irbid, 211-63, Jordan
ma@yu.edu.jo,

N_s, N_S The equivalent number of turns of the q-axis and d-axis stator windings, respectively.

L_{ls}, L_{ms} The leakage inductance and the magnetizing inductance the q-axis stator winding, respectively.

L_{lS}, L_{mS} The leakage inductance and the magnetizing inductance of the d-axis stator winding, respectively.

L'_{lr}, L'_{lR} The leakage inductance and magnetizing inductance of the d-axis rotor winding referred to stator windings, respectively.

J The inertia constant of the rotor and load.

B_m The damping coefficient of the motor and mechanical load.

P The number of poles.

ω_r The angular rotor speed.

ω_s The angular synchronous speed.

f_s The supply frequency.

C The capacitance in the TCSC.

L The inductance in the TCSC.

X_C The reactance of the of TCSC capacitor.

X_e The equivalent reactance of the TCSC.

v_{TCSC} The voltage the TCSC capacitor.

v_L The voltage the TCSC inductor .

v_{source} The voltage of supply.

T_e The developed electromagnetic torque of the motor.

T_L The mechanical torque of the load.

T_d The damping torque of the load.

2. Introduction

Single-phase induction motor (SPIM) is widely used in low – fractional or subfractional horsepower – power applications. At homes, it is used more than any other type of motors and many industrial applications find this motor a popular choice [1–9]. Its rugged structure and inexpensive cost make this motor very popular. Unfortunately, this motor does not have the capability to run directly, as it is not a self-starting motor. Therefore, this motor should initially be operated as a two-phase motor by auxiliary means [1]. The SPIM generally has a main winding and an auxiliary winding and a squirrel-cage rotor.

The most common types of two-winding SPIM are the split-phase, capacitor-start, capacitor-run, and capacitor-start capacitor-run. Except the split-phase SPIM, the two-winding SPIM uses auxiliary capacitor [1–3]. A two-phase motor operation is traditionally achieved by using inductive or capacitive auxiliary windings. If an inductive auxiliary winding is used, a split-phase motor operation is obtained. The motor can also operate as a capacitor-start motor or a capacitor-start capacitor-run motor by adding appropriate capacitors to the auxiliary winding to get more phase shift relative to main winding. Capacitor values are discrete values selected by a designer and added to motor by a manufacturer. The capacitors are connected or disconnected to the auxiliary winding of the

motor through a mechanical centrifugal switch. Figure 1 shows a schematic diagram of the traditionally used capacitor-start capacitor-run SPIM.

In the capacitor-start SPIM, a large capacitance value is used during starting period to get higher starting torque and to enhance running performance we disconnect the capacitor after the motor speed reaches about 75% of synchronous speed. To improve the starting torque, efficiency, and running performance of a capacitor-start capacitor-run motor, the two parallel capacitors are connected during the starting period (to improve starting torque) and when the motor speed reaches nearly 75% of synchronous speed one capacitor is disconnected by a centrifugal switch, leaving one smaller capacitor connected to the auxiliary winding to enhance the running performance.

Problems, modeling, simulation and control of single-phase induction motors have received a great deal of attention in the literature over the last few decades. A considerable recent effort and research have been directed towards providing an optimal performance of the motor for a wide range of machine operating conditions [7–21]. In [7–10] different proposals have been presented to adjust the auxiliary capacitors using electronic switches. Recent research was also focused on adjustable-speed operation [11], low-cost-topologies [12], vector control [13, 14], space-vector modulation techniques [15, 16], sensorless control [17, 18], energy-saving schemes [19] and optimization [20, 21].

Flexible AC Transmission System (FACTS) devices have been newly developed and utilized in some developed countries [22–26]. FACTS devices, whose operations are realized using advanced quick-response power electronic components, are capable of providing the required flexibility to operate the system in which FACTS devices are equipped. Their instant response to control inputs grants a high ability to enhance transient and steady-state operations of the system.

Armed with a high speed switching capability, fast boosting of its degree of compensation, reduced weight, and decreased space requirements, the TCSC integrates a broad range of positive technical qualifications as it considerably provides control of voltage, impedance and phase angle, which are basic parameters on which electric system performance depends [27–32]. The series compensation is mainly based on the idea of adjusting impedance of line in which it is inserted, where the thyristors in TCSC are used to switch a variable series capacitance/inductance into the circuit.

For the reason that the TCSC can change its impedance quickly as firing angle is controlled, this paper proposes to use the TCSC as variable capacitor to improve starting torque and enhance running performance of SPIM. Figure 2 shows a schematic diagram of the proposed TCSC-Operated SPIM. As shown in this figure, a TCSC is inserted in the auxiliary winding of the SPIM as a replacement of the traditional auxiliary component and the accompanying mechanical centrifugal switch.

The definitions of the parameters and variables used in this paper are given in Appendix I

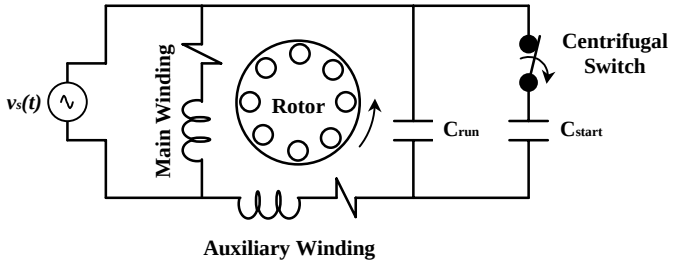

Fig. 1: Schematic diagram of a capacitor-start capacitor-run SPIM

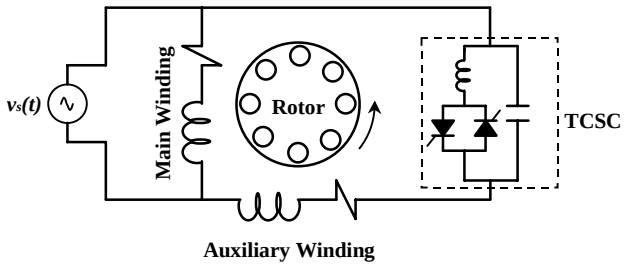

Fig. 2: Schematic diagram of the proposed TCSC-operated SPIM

2. Mathematical Model of TCSC

The equivalent circuit of TCSC is shown in Figure 3, with resistances have been neglected [27–32]. As shown in the figure, the TCSC consists of a capacitor connected in a parallel thyristor-controlled inductor. TCSC operates such that the TCSC is seen by the circuit in which it is inserted as, virtually, having an increased reactance beyond the original reactance of the of TCSC capacitor (X_C), i.e., the TCSC is seen as controllable equivalent reactance. The currents i, i_C and i_L in Figure 3 represent, respectively, the total current, the capacitor's current and the inductor's current of the TCSC. The voltages of the capacitor and the inductor of the TCSC are denoted by v_C and v_L, respectively.

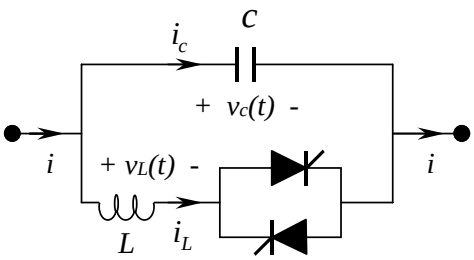

Fig. 3: Equivalent circuit of the TCSC.

The TCSC has two modes of operation, which are TCSC with TRIAC is ON and TCSC with TRIAC is OFF. When the TRIAC is ON, the TCSC will appear as parallel LC circuit, where the capacitor and the inductor have the same voltage. The ON mode of operation is described by the following equations:

$$v_C(t) = v_L(t) = L\frac{di_L(t)}{dt} \tag{1}$$

$$i(t) = i_L(t) + i_C(t) \tag{2}$$

$$i_C(t) = C\frac{dv_C(t)}{dt} \tag{3}$$

$$\frac{dv_C(t)}{dt} = \frac{1}{C}(i(t) - i_L(t)) \tag{4}$$

$$\frac{di_L(t)}{dt} = \frac{v_C(t)}{L} \tag{5}$$

When the TRIAC is OFF, the inductor is open and the TCSC will appear as a capacitor, therefore, the current $i(t)$ will pass through the capacitor only. In this mode of operation, the TCSC is modeled by the following equations:

$$v_c(t) = \frac{1}{C}\int i\ dt \tag{6}$$

$$i(t) = i_C(t) = C\frac{dv_C(t)}{dt} \tag{7}$$

$$i_L(t) = 0 \tag{8}$$

In nutshell, we can consider TCSC circuit as a parallel LC circuit with a variable inductance. For SPIM operations, because in starting and running periods we need capacitive impedances to be connected to the auxiliary winding of the SPIM, we select the values of L and C in this paper such that a capacitive impedance of TCSC is obtained all the time, i.e., the inductive impedance is selected such that it is greater than the capacitive impedance in the parallel LC circuit.

3. Mathematical Models of SPIM and TCSC-Operated SPIM

3.1. Mathematical Model of SPIM

The mathematical model of SPIM in terms of stationary reference-frame variables is given by the following equations [2, 3, 8, 9]:

$$v_{qs} = r_s i_{qs} + \frac{d(\lambda_{qs})}{dt} \tag{9}$$

$$v_{ds} = r_S i_{ds} + \frac{d(\lambda_{ds})}{dt} \tag{10}$$

$$v'_{qr} = r'_r\, i'_{qr} - a_{sS}\, \omega_r \lambda'_{dr} + \frac{d(\lambda'_{qr})}{dt} \tag{11}$$

$$v'_{dr} = r'_r\, i'_{dr} + a_{Ss}\, \omega_r \lambda'_{qr} + \frac{d(\lambda'_{dr})}{dt} \tag{12}$$

where $a_{sS} = N_s / N_S$ and $a_{Ss} = N_S / N_s$. If $v'_{qr} = v'_{dr} = 0$, the set of dynamic equations representing the SPIM, which are given by (9)–(12), can be represented by the equivalent circuits shown in Figure 4 [2].

In matrix form, the equation (9)–(12) can be expressed as:

$$\begin{bmatrix} v_{qs} \\ v_{ds} \\ v'_{qr} \\ v'_{dr} \end{bmatrix} = \begin{bmatrix} r_s & 0 & 0 & 0 \\ 0 & r_S & 0 & 0 \\ 0 & 0 & r'_r & 0 \\ 0 & 0 & 0 & r'_r \end{bmatrix} \begin{bmatrix} i_{qs} \\ i_{ds} \\ i'_{qr} \\ i'_{dr} \end{bmatrix} + \frac{d}{dt} \begin{bmatrix} \lambda_{qs} \\ \lambda_{ds} \\ \lambda'_{qr} \\ \lambda'_{dr} \end{bmatrix} + \begin{bmatrix} 0 & 0 & 0 & 0 \\ 0 & 0 & 0 & 0 \\ 0 & 0 & 0 & -a_{sS}\omega_r \\ 0 & 0 & a_{sS}\omega_r & 0 \end{bmatrix} \begin{bmatrix} \lambda_{qs} \\ \lambda_{ds} \\ \lambda'_{qr} \\ \lambda'_{dr} \end{bmatrix} \tag{13}$$

In (9)–(13), the flux linkages of stator and rotor are defined as:

$$\lambda_{qs} = L_{ls} i_{qs} + L_{ms}(i_{qs} + i'_{qr}) \tag{14}$$

$$\lambda_{ds} = L_{lS} i_{ds} + L_{mS}(i_{ds} + i'_{dr}) \tag{15}$$

$$\lambda'_{qr} = L'_{lr}\, i'_{qr} + L_{ms}(i_{qs} + i'_{qr}) \tag{16}$$

$$\lambda'_{dr} = L'_{lR}\, i'_{dr} + L_{mS}(i_{ds} + i'_{dr}) \tag{17}$$

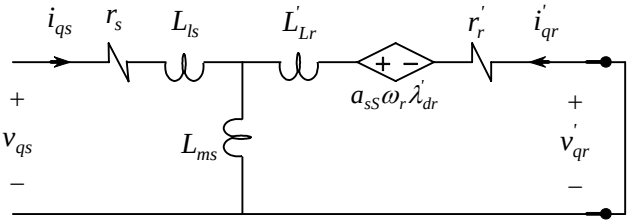

(a) The q-axis equivalent circuits

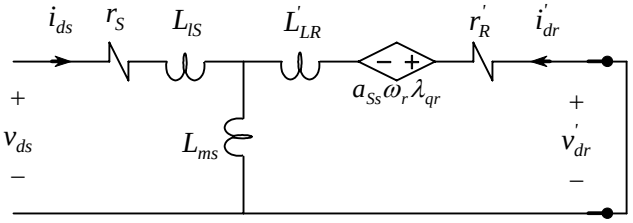

(b) The d-axis equivalent circuits

Fig. 4: The equivalent circuits of a SPIM in terms of stationary reference frame

By substituting the expressions of flux linkages of (14)–(17) in (13) and with $v_{qs} = v_{ds} = v_{source}$ and $v'_{qr} = v'_{dr} = 0$, the model of the SPIM in state-space matrix form is given by:

$$\begin{bmatrix} v_{qs} \\ v_{ds} \\ 0 \\ 0 \end{bmatrix} = \begin{bmatrix} L_{ls}+L_{ms} & 0 & L_{ms} & 0 \\ 0 & L_{lS}+L_{mS} & 0 & L_{mS} \\ L_{ms} & 0 & L'_{lr}+L_{ms} & 0 \\ 0 & L'_{lR} & 0 & L'_{lR}+L_{mS} \end{bmatrix} \frac{d}{dt} \begin{bmatrix} i_{qs} \\ i_{ds} \\ i'_{qr} \\ i'_{dr} \end{bmatrix} + \begin{bmatrix} r_s & 0 & 0 & 0 \\ 0 & r_S & 0 & 0 \\ 0 & 0 & r'_r & 0 \\ 0 & 0 & 0 & r'_R \end{bmatrix} \begin{bmatrix} i_{qs} \\ i_{ds} \\ i'_{qr} \\ i'_{dr} \end{bmatrix} + \omega_r \begin{bmatrix} 0 & 0 & 0 & 0 \\ 0 & 0 & 0 & 0 \\ 0 & -a_{sS}L_{mS} & 0 & -a_{sS}\left(L'_{lR}+L_{mS}\right) \\ a_{Ss}L_{ms} & 0 & a_{Ss}\left(L'_{lr}+L_{ms}\right) & 0 \end{bmatrix} \begin{bmatrix} i_{qs} \\ i_{ds} \\ i'_{qr} \\ i'_{dr} \end{bmatrix} \quad (18)$$

In (18), the voltage v_{qs} and v_{ds} are given by:

$$v_{qs} = v_{ds} = v_{source} \quad (19)$$

where $v_{source} = V_m \cos(\omega_s t)$ and $\omega_s = 2\pi f_s$.

3.2. Mathematical Model of TCSC-Operated SPIM

For the case when TRIAC is OFF, the q-axis equivalent circuit of the SPIM remains the same as that of the uncompensated SPIM which was shown previously in Figure 4a, but the d-axis equivalent circuit of the SPIM is modified to include the capacitor C as shown in Figure 5. The voltage v_{ds} and the state variable v_{TCSC} can be expressed as:

$$v_{ds} = v_{source} - v_{TCSC} \quad (20)$$

$$i_{ds} = C\frac{dv_{TCSC}}{dt} \quad (21)$$

By adding the equations of v_{ds} and v_{TCSC} state variables of (20) and (21) to the SPIM equations given by (18), the model of the TCSC-operated SPIM, with TRIAC is OFF, can be described by the following equation:

$$\begin{bmatrix} v_{source} \\ v_{source} \\ 0 \\ 0 \\ 0 \end{bmatrix} = \begin{bmatrix} L_{ls}+L_{ms} & 0 & L_{ms} & 0 & 0 \\ 0 & L_{lS}+L_{mS} & 0 & L_{mS} & 0 \\ L_{ms} & 0 & L'_{lr}+L_{ms} & 0 & 0 \\ 0 & L'_{lR} & 0 & L'_{lR}+L_{mS} & 0 \\ 0 & 0 & 0 & 0 & 1 \end{bmatrix} \frac{d}{dt} \begin{bmatrix} i_{qs} \\ i_{ds} \\ i'_{qr} \\ i'_{dr} \\ v_{TCSC} \end{bmatrix} + \begin{bmatrix} r_s & 0 & 0 & 0 & 0 \\ 0 & r_S & 0 & 0 & 1 \\ 0 & 0 & r'_r & 0 & 0 \\ 0 & 0 & 0 & r'_R & 0 \\ 0 & -1/C & 0 & 0 & 0 \end{bmatrix} \begin{bmatrix} i_{qs} \\ i_{ds} \\ i'_{qr} \\ i'_{dr} \\ v_{TCSC} \end{bmatrix} + \omega_r \begin{bmatrix} 0 & 0 & 0 & 0 & 0 \\ 0 & 0 & 0 & 0 & 0 \\ 0 & -a_{sS}L_{mS} & 0 & -a_{sS}\left(L'_{lR}+L_{mS}\right) & 0 \\ a_{Ss}L_{ms} & 0 & a_{Ss}\left(L'_{lr}+L_{ms}\right) & 0 & 0 \\ 0 & 0 & 0 & 0 & 0 \end{bmatrix} \begin{bmatrix} i_{qs} \\ i_{ds} \\ i'_{qr} \\ i'_{dr} \\ v_{TCSC} \end{bmatrix} \quad (22)$$

For the case when TRIAC is ON, the q-axis equivalent circuit of the SPIM also remains the same as that of the uncompensated SPIM (see Figure 4a), but the d-axis equivalent

circuit of the SPIM is modified to include the LC parallel circuit as shown in Figure 6. The state variables i_L and v_{TCSC} can be expressed as:

$$i_L = i_{ds} - C\frac{dv_{TCSC}}{dt} \tag{23}$$

$$v_{TCSC} = L\frac{di_L}{dt} \tag{24}$$

By adding the equations of the voltage v_{ds} (which is also given by (20)) and i_L and v_{TCSC} state variables of (23) and (24) to the SPIM equations given by (18), the model of the TCSC-operated SPIM, with TRIAC is ON, can be described by the following equation:

$$\begin{bmatrix} v_{source} \\ v_{source} \\ 0 \\ 0 \\ 0 \\ 0 \end{bmatrix} = \begin{bmatrix} L_{ls}+L_{ms} & 0 & L_{ms} & 0 & 0 & 0 \\ 0 & L_{lS}+L_{mS} & 0 & L_{mS} & 0 & 0 \\ L_{ms} & 0 & L'_{lr}+L_{ms} & 0 & 0 & 0 \\ 0 & L'_{lR} & 0 & L'_{lR}+L_{mS} & 0 & 0 \\ 0 & 0 & 0 & 0 & 1 & 0 \\ 0 & 0 & 0 & 0 & 0 & 1 \end{bmatrix} \frac{d}{dt} \begin{bmatrix} i_{qs} \\ i_{ds} \\ i'_{qr} \\ i'_{dr} \\ v_{TCSC} \\ i_L \end{bmatrix}$$

$$+ \begin{bmatrix} r_s & 0 & 0 & 0 & 0 & 0 \\ 0 & r_S & 0 & 0 & 1 & 0 \\ 0 & 0 & r'_r & 0 & 0 & 0 \\ 0 & 0 & 0 & r'_R & 0 & 0 \\ 0 & -1/C & 0 & 0 & 0 & 1/C \\ 0 & 0 & 0 & 0 & -1/L & 0 \end{bmatrix} \begin{bmatrix} i_{qs} \\ i_{ds} \\ i'_{qr} \\ i'_{dr} \\ v_{TCSC} \\ i_L \end{bmatrix} \tag{25}$$

$$+ \omega_r \begin{bmatrix} 0 & 0 & 0 & 0 & 0 & 0 \\ 0 & 0 & 0 & 0 & 0 & 0 \\ 0 & -a_{sS}L_{mS} & 0 & -a_{sS}\left(L'_{lR}+L_{mS}\right) & 0 & 0 \\ a_{Ss}L_{ms} & 0 & a_{Ss}\left(L'_{lr}+L_{ms}\right) & 0 & 0 & 0 \\ 0 & 0 & 0 & 0 & 0 & 0 \\ 0 & 0 & 0 & 0 & 0 & 0 \end{bmatrix} \begin{bmatrix} i_{qs} \\ i_{ds} \\ i'_{qr} \\ i'_{dr} \\ v_{TCSC} \\ i_L \end{bmatrix}$$

The expression of instantaneous electromagnetic torque and the equation of electromechanical system of SPIM, for both uncompensated SPIM and TCSC-operated SPIM, are given by [2, 3]:

$$T_e = \frac{P}{2}\left(a_{Ss}\,\lambda'_{qr}\,i'_{dr} - a_{sS}\,\lambda'_{dr}\,i'_{qr}\right) \tag{26}$$

$$\frac{d\omega_r}{dt} = \frac{(P/2)}{J}\left(T_e - T_L - T_d\right) \tag{27}$$

The damping torque of the load (T_d) in (27) is given by:

$$T_d = B_m\omega_r \tag{28}$$

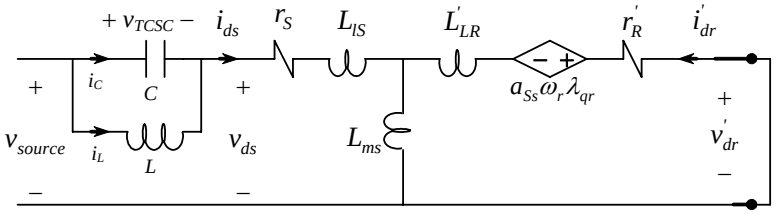

Fig. 5: The d-axis equivalent circuits of a TCSC-Operated SPIM when the TRIAC is ON

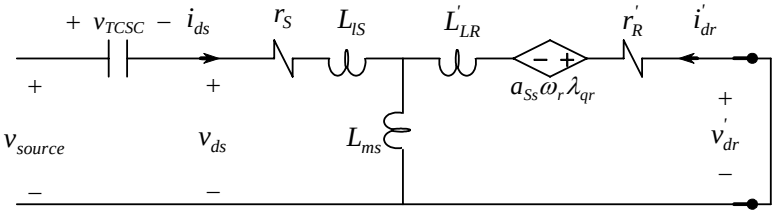

Fig. 6: The d-axis equivalent circuits of a TCSC-Operated SPIM when the TRIAC is OFF

4. Simulation Results

The nonlinear differential equations, which describe the SPIM dynamic behavior, have been simulated on a computer using the MATLAB software package. In this paper we use a 0.25 hp, 4-pole, 60 Hz, 110 V SPIM with $J = 1.46 \times 10^{-2}$ $kg.m^2$, $B_m = 0$ and (N_S / N_s)=1.18. The machine parameters are as follow:

Stator parameters:

r_s = 2.02 Ω, r_S = 7.14Ω, X_{ls} = 2.79Ω, X_{lS} = 3.22 Ω , X_{ms} = 66.8Ω , X_{mS} = 92.9Ω

Rotor parameter:

r'_r = 4.12Ω , r'_R = 5.74Ω , X'_{lr} = 2.12Ω , X'_{lR} = 2.95Ω

TCSC parameters:

X_L =15.83 Ω, X_C =14.5Ω

The transient response of the free acceleration (no-load) of the traditional capacitor-start capacitor-run SPIM (see Figure 1) are shown in Figure 7. From this figure we can notice that the motor has relatively a good starting torque and acceleration time since the equivalent capacitor is high at starting.

To show the advantageous features and capabilities the TCSC may bring to the SPIM operation during starting and running periods, we next consider the effect of the TCSC on the motor at many starting firing angles at starting period. After the motor reaches 75% of its synchronous speed the TCSC firing angle is set equal to zero to obtain a high speed and a better running torque.

The same free acceleration (no-load) characteristics of the traditional capacitor-start capacitor-run SPIM can be obtained by setting the starting firing angle at 180^o as shown in Figure 8. The slight increase in the starting torque (compared to Figure 7) is due to neglecting the resistance of the capacitor in the TCSC modeling.

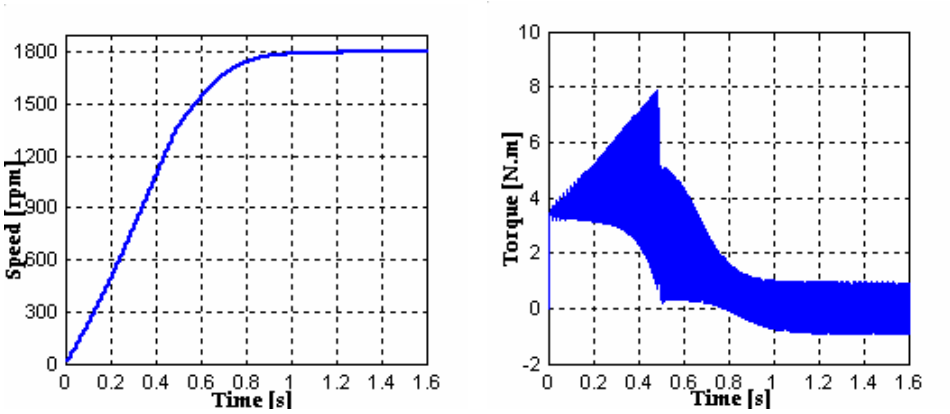

Fig. 7: The instantaneous speed and torque of capacitor-start capacitor-run SPIM.

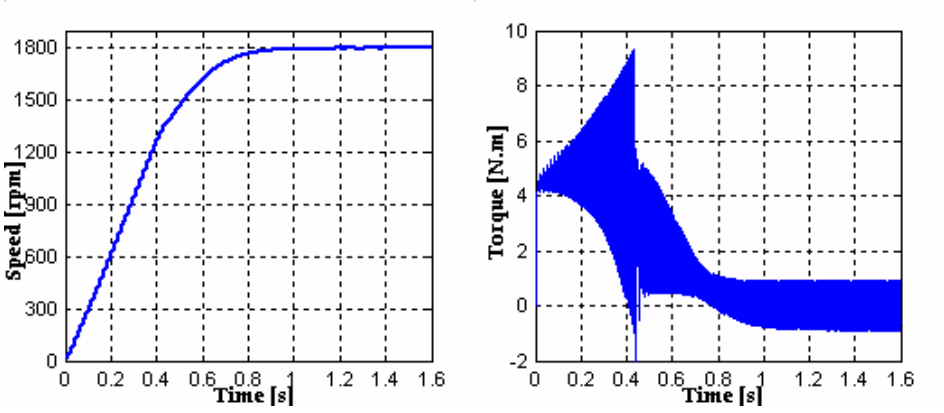

Fig. 8: The instantaneous speed and torque of SPIM with TCSC.

The impacts of selecting different starting firing angles on free acceleration starting torque are shown in Figure 9. At 160^o firing angle (Figure 9a), the starting torque is 4.5 N.m and at 90^o firing angle (Figure 9b), the starting torque is about 3.5 N.m. If we consider a small firing angle such as 30^o (Figure 9c), we notice that the starting torque is less than 2 N.m.. Therefore, as we increase the firing angle the starting torque will increase and that is expected because the equivalent capacitance increases as the firing angle increases.

The effect of different starting firing angles is not significant on speed characteristic as in the cases of the running firing angle, especially for close values of firing angles, but the starting firing angle affects the acceleration time. Figure 10 shows that the motor needs different time to reach 90% of synchronous speed, which equals 1620 rpm. Time required to reach this speed at each of 180^o, 150^o, 90^o and 30^o firing angles is summarized in table 1.

All previous simulation results of the TCSC-Operated SPIM, have shown the effect of the starting firing angle on motor performance with 0^o running firing angle, which achieves the best running performance. To get a variable speed drive, i.e., if the motor is desired to work under another speed we may change the running firing angle. Figure 11 represents the free-acceleration speed characteristics dynamic behavior of TCSC-SPIM with 150^o starting firing angle and 180^o running firing angle. As can be seen from this figure, the steady-state speed will decrease to 1700 rpm.

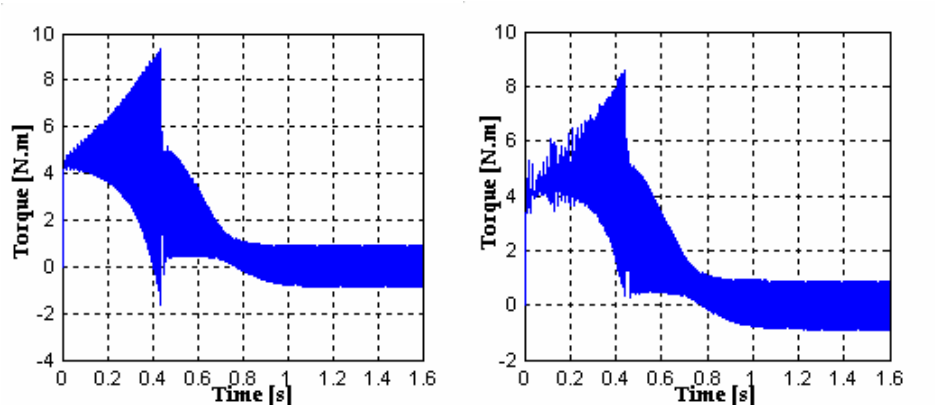

(a) 160^{o} firing angle.

(b) 90^{o} firing angle.

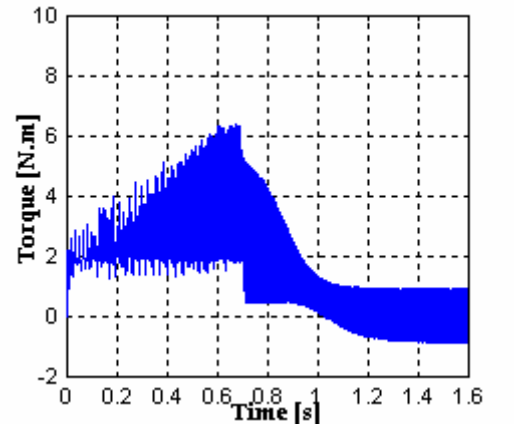

(c) 30^{o} firing angle.

Fig. 9: The instantaneous electromagnetic torque at 160^{o}, 90^{o} and 30^{o} firing angles.

Table 1: Time Elapsed to Reach 90% of Synchronous Speed

Firing Angle	Time
180^{0}	0.5971
150^{o}	0.6002
90^{o}	0.6016
30^{o}	0.8513

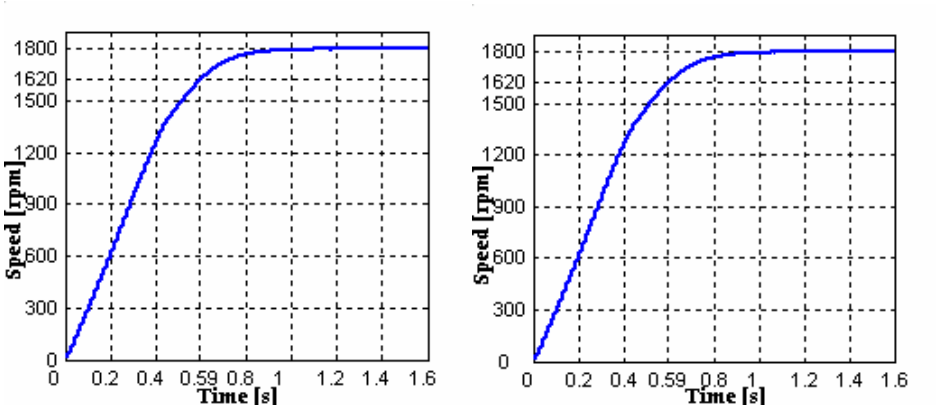

(a) 180^o firing angle.

(b) 150^o firing angle.

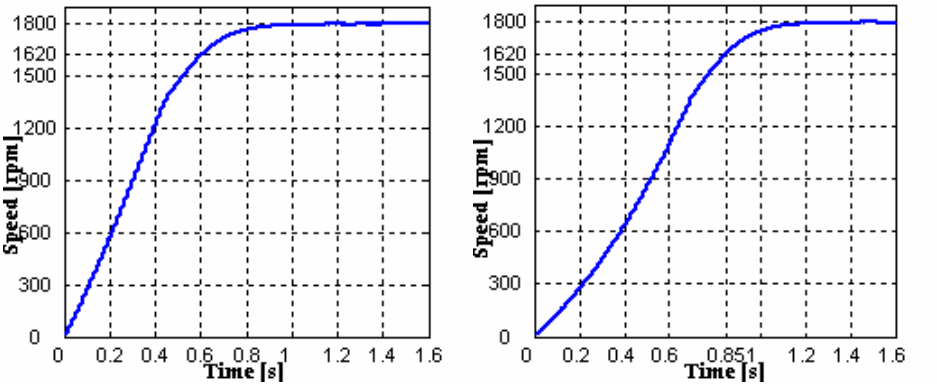

(c) 90^o firing angle.

(d) 30^o firing angle.

Fig. 10: The speed-time characteristics at 180^o, 150^o, 90^o and 30^o firing angles.

The torque and speed characteristics, with $T_L = 1\ N.m.$, for both the traditional capacitor-start capacitor-run SPIM and the TCSC-operated SPIM are shown in figs. 12 and 13, respectively. For both cases, the load has been applied at $t = 1\ sec$. As can be noticed from comparing the two figures, the TCSC also works effectively in starting and running periods and may do the functions of the starting and running capacitors in the traditional motor operation.

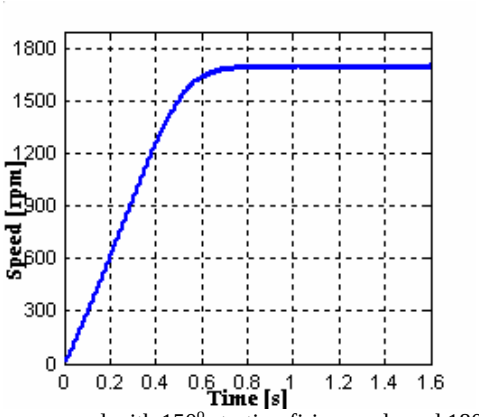

Fig. 11: The instantaneous speed with 150^{o} starting firing angle and 180^{o} running firing angle

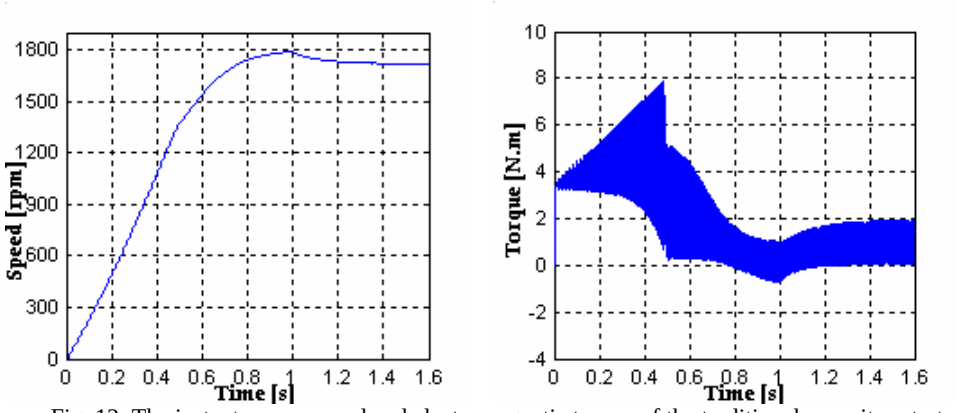

Fig. 12: The instantaneous speed and electromagnetic torque of the traditional capacitor-start capacitor-run loaded SPIM

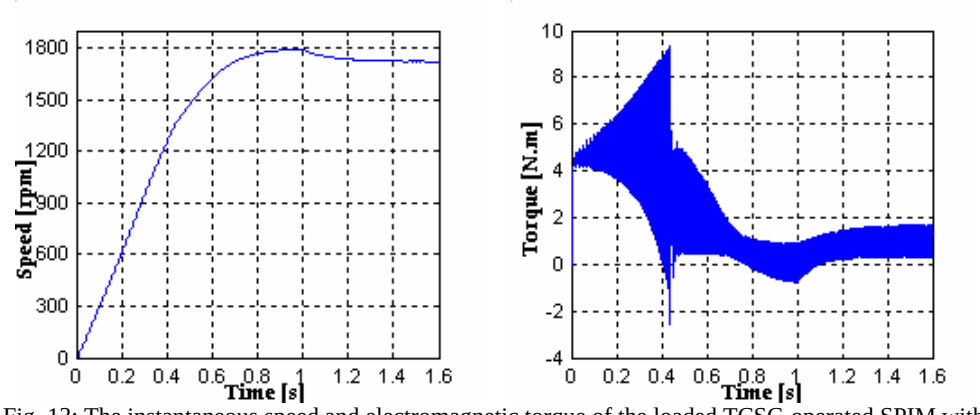

Fig. 13: The instantaneous speed and electromagnetic torque of the loaded TCSC-operated SPIM with 180^{o} starting firing angle and 0^{o} running firing angle

5. Conclusions

In this paper we have represented a TCSC as variable capacitor that can replace the traditionally used double capacitors for starting and running operations in SPIM. In addition, the paper has presented the mathematical state-space model of the TCSC-operated

SPIM. The dynamic characteristics of SPIM using TCSC for different controllable firing angles have been discussed in the paper. The effects of firing angle of the TCSC on the starting and steady-state operations have also been investigated.

In this paper we represent that TCSC- operated SPIM can simply be used as capacitor-start capacitor-run SPIM with 180^o starting firing angle and 0^o running firing angle. By taking the benefits of TCSC as variable capacitor we can accomplish the desired characteristics in both starting and running periods by the controllable firing angle.

As related to effect of the firing angle on starting torque, the simulation results showed that increasing the starting firing angle would result in an increase (improvement) in the starting torque because the equivalent starting capacitance increased as the firing angle increased. From speed-time characteristics illustrated in the paper, the characteristics showed that the time required to reach a certain speed would increase as the firing angle was decreased.

References

[1] S. J. Chapman, Electric Machinery Fundamentals, WCB/McGraw-Hill, 1999.

[2] P. C. Krause, O. Wasynszuk and S.D. Sudhoff, Analysis of Electric Machinery, New York: IEEE Press, 1995.

[3] C.M. Ong, Dynamic Simulation of Electric Machinery using Matlab/Simulink, New Jersey: Prentice Hall PTR, 1998.

[4] M. B. Correa, C. B. Jacobina, A. M. Lima, and E. R. Silva, Rotor-Flux-Oriented Control of a Single-Phase Induction Motor Drive, IEEE Trans. Industrial Electronics, Vol. 47, No.4, 2000, pp. 832-841.

[5] E. R. Collins Jr., A. B. Puttgen, and W. E. Sayle II, Single-phase induction motor adjustable speed drive: Direct phase angle control of the auxiliary winding supply, Conf. Rec. IEEE-IAS Annu. Meeting, 1988, pp. 246–252.

[6] F. Neves, R. Landim, E. Filho, Z. Lins, J. Cruz, S. Silva and B. Menezes, Direct Torque Control Strategies Four Single-Phase Induction Motor Drives, 14th Congresso Brasileiro de Automatica, 2002, pp. 1961-1966.

[7] A. Lettenmaier, D.W. Novotny, T. and T. A. Lipo, Single-phase induction motor with an electronically controlled capacitor, IEEE Trans. Industrial Applications, Vol. 27, No. 1, 1991, pp. 38–43.

[8] S. Sunter, M. Ozdemir and B. Gumus, Modeling And Simulation of a Single Phase Induction Motor With Adjustable Switched Capacitor, 9th International Conference On Power Electronic and Motion Control-WPE-PEMC 2000 Kosice, 2000, 1-5.

[9] S. Sunter M. Ozdemir and B. Gumus, Dynamic Performance of Single-Phase Induction Motor with Switched Capacitor, ELECO'99, Bursa,1999, pp. 367-370.

[10] T. Liu, A Maximum Torque Control with a Controlled Capacitor for a Single-Phase Induction Motor, IEEE Trans. Industrial Electronics, Vol. 42, No. 1, 1995, pp. 17-24.

[11] M. Chomat and T.A. Lipo, Adjustable-Speed Single-Phase IM Drive With Reduced Number of Switches, IEEE Trans. Ind. Appl., Vol. 39, No. 3, 2003, pp. 819–825.

[12] F. Blaabjerg, F. Lungeanu, K. Skaug, and M. Tonnes, Two-Phase Induction Motor Drives Low-Cost Topologies for TPIM Drives in Industrial Applications, IEEE Trans. Industrial Applications Magazine, Vol. 10, No. 4, 2004, pp. 24–32. 2004.

[13] S. Reicy and S. Vaez-Zadeh, Vector Control of Single-Phase Induction Machine With Maximum Torque Operation, Proc. ISIE, 2005, Vol. 3, pp. 923–928.

[14] M. R. Correa, C. B. Jacobina, E. R. C.D. Silva, and A.M.N. Lima, Vector Control Strategies for Single-Phase Induction Motor Drive Systems, IEEE Trans. Ind. Electron., Vol. 51, No. 5, 2004, pp. 1073–1080.

[15] D. H. Jang and D. Y. Yoon, Space-Vector PWM technique for Two-Phase Inverter-Fed Two Phase Induction Motors, IEEE Trans. Ind. Appl., Vol. 39, No. 2, 2003, pp. 542–549.

[16] M. A. Jabbar, A. M. Khambadkone, and Z. Yanfeng, Space-Vector Modulation in a Two-Phase Induction Motor Drive for Constant-Power Operation, IEEE Trans. Ind. Electron., Vol. 51, No. 5, 2004, pp. 1081–1088.

[17] M. B. R. Correa, C. B. Jacobina, P. M. dos Santos, E. C. dos Santos, and A. M. N. Lina, Sensorless IFOC for Single-Phase Induction Motor Drive System, Proc. EEE Int. Conf. Electr.Mach. Drives, 2005, pp. 162–166.

[18] S. Vaez-Zadeh and A. Payman, Design and Analysis of Sensorless Torque Optimization for Single Phase Induction Motors, Proc. Int. J. Energy Conver. Manage., 2006, Vol. 47, pp.1464–1477.

[19] K . Sundaresswaren, An Improved Energy-Saving Scheme for Capacitor-Run Induction Motor, IEEE Trans. Ind. Electronics, Vol. 48, 2001, pp. 238-240.

[20] C. Mademlis, I. Kioskeridis, and T. Theodoulidis, Optimization of Single-Phase Motors, Part 1: Maximum Energy Efficiency Control, *IEEE Trans.Energy Convers.*, Vol. 20, No. 1, 2005, pp. 187–195.

[21] C. Mademlis, I. Kioskeridis, and T. Theodoulidis, Optimization of Single-Phase Motors, Part 2: Maximum Energy Efficiency Control," *IEEE Trans.Energy Convers.*, Vol. 20, No. 1, 2005, pp. 196–203.

[22] N. G. Hingoran, & L. Gyugyi, Understanding FACTS, IEEE Press, 2000.

[23] Y. H. Song, & A. Johns, Flexible AC Transmission Systems (FACTS), IEE , 1999.

[24] N. H. Hignorani, Flexible AC transmission systems, IEEE Spectrum, April 1993, pp. 40–45.

[25] A.S. Edris, M. Mehraban, L. Rahman, S.A. Gyugyi and T. Reitman, Controlling the Flow of Real and Reactive Power, IEEE Computer Applications in Power, 1998, pp. 20-25.

[26] D.J. Gotham, & G.T. Heydt, Power Flow Control and Power Flow Studies for Systems with FACTS Devices, IEEE Trans. Power Systems, Vol. 13, No. 1, 1998, pp. 60-65.

[27] M. Noroozian, L. Angquist, M. Ghandhari and G. Anderson, Improving Power System Dynamics by Series-connected FACTS Devices, IEEE Trans. Power Delivery, Vol. 12, No. 4, 1997.

[28] H. G. Han J.K. Park, Analysis Operation Modes of Thyristor Controlled Series Compensators Using State Space Analysis, 29th IEEE Power Electronics Specialists Conference (PESC 98), May 98, pp. 829-834.

[29] A.D. Del Rosso, C.A. Canizares, and V.M. Dona, A Study of TCSC Controller Design for Power System Stability Improvement, *IEEE Trans. Power Syst*., Vol. 18, No. 4, 2003, pp.1487-1496.

[30] S. Panda, R. N. Patel, N. P. Padhy, Power System Stability Iimprovement by TCSC Controller Employing a Multi-Objective Genetic Algorithm Approach, *Int. J. Intelligent Tech.* , Vol. 1, No. 4, 2006, pp.266-273.

[31] S. Panda and N.P. Padhy, Thyristor Controlled Series Compensator Based Controller Design Employing Genetic Algorithm: A Comparative Study, *Int. J. Elect. , Circuits and Syst.*, Vol.1, No.1, 2007, pp. 38-47.

[32] S. Panda, and N.P. Padhy, MATLAB/SIMULINK Based Model of Single-Machine Infinite-Bus with TCSC for Stability Studies and Tuning Employing GA, *Int. J. Computer Sci. and Eng.* , Vol. 1, No. 1, 2007, pp. 50-59.